Metal Halide Perovskite Polycrystalline Films Exhibiting Properties of Single Crystals

Joule

CellPress

Article

Metal Halide Perovskite Polycrystalline Films Exhibiting Properties of Single Crystals

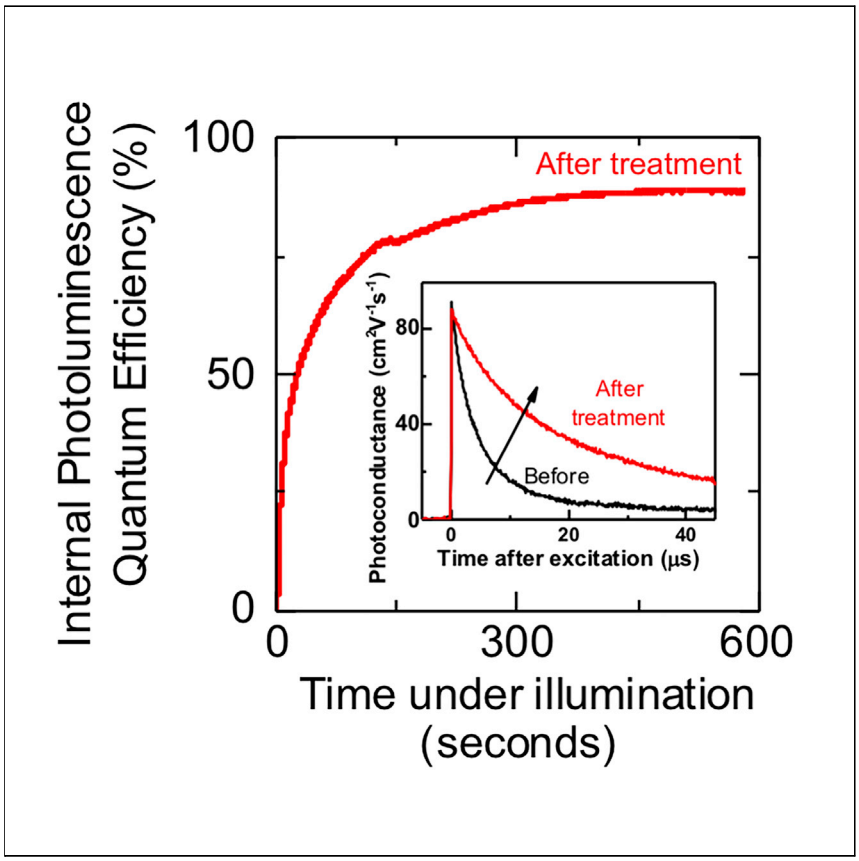

The authors demonstrate the use of light and atmospheric treatments on polycrystalline perovskite thin films, resulting in properties approaching those of the best crystalline semiconductors reported to date. The results translate to exceptional photovoltaic device performances with rapid rises to stabilized power output consistent with an inhibition of ionic migration.

Roberto Brenes, Dengyang Guo, Anna Osherov, ..., Vladimir Bulović, Tom J. Savenije, Samuel D. Stranks

sds65@cam.ac.uk

HIGHLIGHTS

Internal photoluminescence quantum efficiency of perovskite films reaching 89%

Carrier lifetimes in passivated perovskite films of 32 μs

Solar cell efficiencies of 19.2% with near-instant rise to stable power output

Mechanism proposed based on elimination of shallow surface states

Brenes et al., Joule *1*, 155–167
September 6, 2017
Published by Elsevier Inc.
http://dx.doi.org/10.1016/j.joule.2017.08.006

Joule

CellPress

Article

Metal Halide Perovskite Polycrystalline Films Exhibiting Properties of Single Crystals

Roberto Brenes,[1] Dengyang Guo,[2] Anna Osherov,[1] Nakita K. Noel,[3] Christopher Eames,[4] Eline M. Hutter,[2] Sandeep K. Pathak,[1,3] Farnaz Niroui,[1] Richard H. Friend,[5] M. Saiful Islam,[4] Henry J. Snaith,[3] Vladimir Bulović,[1] Tom J. Savenije,[2] and Samuel D. Stranks[1,5,6,*]

SUMMARY

Metal halide perovskites are generating enormous excitement for use in solar cells and light-emission applications, but devices still show substantial non-radiative losses. Here, we show that by combining light and atmospheric treatments, we can increase the internal luminescence quantum efficiencies of polycrystalline perovskite films from 1% to 89%, with carrier lifetimes of 32 μs and diffusion lengths of 77 μm, comparable with perovskite single crystals. Remarkably, the surface recombination velocity of holes in the treated films is 0.4 cm/s, approaching the values for fully passivated crystalline silicon, which has the lowest values for any semiconductor to date. The enhancements translate to solar cell power-conversion efficiencies of 19.2%, with a near-instant rise to stabilized power output, consistent with suppression of ion migration. We propose a mechanism in which light creates superoxide species from oxygen that remove shallow surface states. The work reveals an industrially scalable post-treatment capable of producing state-of-the-art semiconducting films.

INTRODUCTION

Metal halide perovskites are an exciting class of materials that possess many of the attributes desirable for optoelectronic applications, with certified power-conversion efficiencies of perovskite-based photovoltaics reaching 22%.[1,2] Despite impressive device performance, perovskites are still far from their full potential. For instance, the photoluminescence quantum efficiency (PLQE) of thin films used in highly efficient devices is still far from unity;[3] typical external PLQE values are ~1% at excitation intensities equivalent to solar illumination, which corresponds to internal PLQE values of ~10% after accounting for losses from photon recycling and poor light out-coupling.[4] These low values are consistent with a sizable density of sub-gap trap states that act as non-radiative recombination centers.[5–7] In order for a solar cell or light-emitting device to reach its theoretical performance limits, luminescence should be maximized with all non-radiative recombination eliminated.[8]

Perovskite single crystals have been reported to exhibit superior properties to polycrystalline thin films, with 2–4 orders of magnitude lower trap densities.[9,10] This leads to long charge-carrier lifetimes and diffusion lengths of tens of microseconds and micrometers, respectively,[11,12] and surface recombination velocities as low as 3 cm/s.[13] However, controlled growth of single crystals into devices does not lend itself to the many advantages offered by solution-processing polycrystalline thin

Context & Scale

Metal halide perovskites are exciting materials for low-cost optoelectronic devices such as solar cells and LEDs. In order to reach the theoretical efficiency limits for both applications, any parasitic non-radiative charge-carrier recombination losses, such as those mediated by carrier trapping, must be eliminated. At present, perovskite materials still suffer from substantial non-radiative decay, particularly under solar illumination conditions, and are therefore yet to reach their full potential. Perovskite single crystals have very low trap concentrations but their controlled growth into devices does not lend themselves to the advantages offered by solution-processing thin films such as roll-to-roll depositions. Here, we demonstrate the use of light and atmospheric treatments on polycrystalline perovskite films, resulting in minimal non-radiative losses and properties approaching those of perovskite single crystals and even the best crystalline semiconductors reported to date.

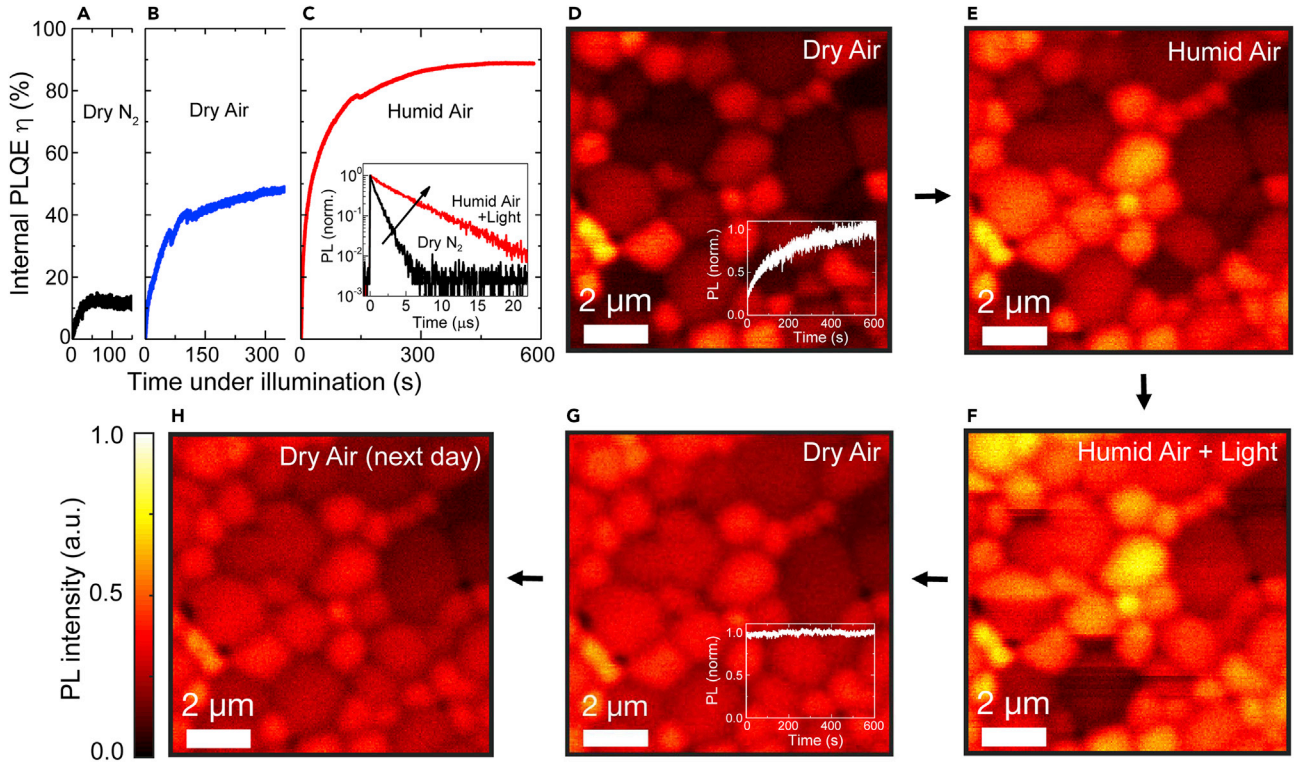

Figure 1. Macro- and Micro-photoluminescence Enhancements of Thin Films under Solar Illumination Conditions

(A–C) Internal PLQE η measurements over time under illumination with a CW 532-nm laser at an excitation intensity equivalent to ~2 sun (~150 mW/cm^2) in dry N_2 (A), dry air (B), and humid air (C). Inset: Time-resolved PL decays of the films after the stated treatment with pulsed excitation at 405 nm (excitation density of 5.4 × 10^{15} cm^{-3}).

(D–H) *In situ* confocal PL maps with 405-nm excitation measured in (D) dry air, (E) humidified air, (F) after light soaking for 10 min under excitation with a 532-nm laser equivalent to ~10 sun under humid air, (G) after returning to dry air, and (H) measured the next day with storage in dry air. Insets to (D) and (G): emission stability of the films in dry air before and after the treatment, respectively, under continuous illumination at 532-nm with intensity equivalent to ~10 sun.

See also Figures S1–S9.

films such as roll-to-roll depositions. Recently, the use of surface treatments to passivate deep trap states in polycrystalline films has been reported, yielding reductions in trap density by an order of magnitude.[14,15] However, it is unclear what impact these surface treatments might have on other properties of the film such as the transport properties, interfacial energies, and grain stability. The illumination of perovskite materials has also been shown to achieve reductions in trap density,[16] and these improvements depend on the light dose[16] and can be boosted further in the presence of oxygen.[17] However, these reports have shown only limited local luminescence enhancements with the effects being reversible on a timescale of ~10 hr and not leading to spatially uniform emission over large areas of a high-quality film. In this work, we use a combination of light and atmospheric post-treatments on methylammonium lead iodide ($MAPbI_3$) perovskite thin films that lead to long-lived and exceptionally large enhancements, with the resulting optoelectronic properties approaching those of single crystals.

RESULTS

Macro- and Micro-photoluminescence Enhancements

Thin films (~250 nm thickness) of $MAPbI_3$ perovskite were solution processed on glass (see Supplemental Information).[18] In Figures 1A–1C, we show the internal

[1]Research Laboratory of Electronics, Massachusetts Institute of Technology, 77 Massachusetts Avenue, Cambridge, MA 02139, USA

[2]Department of Chemical Engineering, Delft University of Technology, van der Maasweg 9, 2629 HZ Delft, the Netherlands

[3]Clarendon Laboratory, University of Oxford, Parks Road, Oxford OX1 3PU, UK

[4]Department of Chemistry, University of Bath, Bath BA2 7AY, UK

[5]Cavendish Laboratory, University of Cambridge, JJ Thomson Avenue, Cambridge CB3 0HE, UK

[6]Lead Contact

*Correspondence: sds65@cam.ac.uk

http://dx.doi.org/10.1016/j.joule.2017.08.006

PLQE values (η) of films in different atmospheric conditions while under continuous-wave (CW) illumination with excitation densities close to solar illumination conditions. The internal values are calculated from the measured external PLQE values (η_{meas}, Figure S1) following the methods of Richter et al.[4] (see Supplemental Information). The film illuminated in dry nitrogen shows a small rise in emission, and the internal PLQE reaches a value of η = 12% (Figure 1A). When the film is instead illuminated in dry air, the photoluminescence (PL) rises substantially and the internal PLQE approaches η = 48% and continues to slowly rise (Figure 1B). When the film is light soaked in humidified air (45% relative humidity), the internal PLQE plateaus at η = 89% (Figure 1C). This is approaching PLQE values in which almost all of the non-radiative decay processes are eliminated, despite starting with internal PLQE values of $\eta \sim$ 1%. We find that the enhancements are retained with only a small drop in PLQE to η = 84% when returning the film to dry air (Figure S1), with the small drop appearing to correlate with the desorption of water molecules from the film surfaces upon drying.[19] We also find corresponding enhancements in carrier lifetime from time-resolved PL measurements (Figure 1C inset), which show radiative bimolecular kinetics (Figure S2).

In Figures 1D–1H, we present a progression of confocal PL maps corresponding to the treatment of light soaking under humidified air (see Figures S3 and S4 for other conditions). Under dry air conditions (Figure 1D), we clearly see a grain-to-grain heterogeneity in emission intensity. There is an increase in the PL baseline intensity when moving to humidified air (Figure 1E), which is consistent with earlier reports of the beneficial effects of humidity on film fabrication.[20,21] However, there is then a substantial increase in intensity of all grains after light soaking for 10 min under excitation with a 532-nm laser at an excitation equivalent to ~10 sun (Figure 1F). When comparing the film after the treatment (Figure 1G) with that before the treatment (Figure 1D), we find that there has been a net increase in the emission intensity, PL lifetime, and spatial homogeneity (Figure S5). Furthermore, there is a near-instant rise to stabilized emission output for the treated film in dry air (Figure 1G inset) compared with the slow rises in the corresponding untreated film under the same conditions (Figure 1D inset). In our recent work, we found a strong correlation between the slow transient PL rises and photo-induced ion migration.[16] Therefore, the elimination of the transient PL rises under illumination suggests that photo-induced ion migration has been inhibited after the treatment.[3] There is a negligible decrease in the enhancements when measured the next day (Figure 1H) and even 3 weeks after treatment when the film is encapsulated with a layer of the polymer poly(methylmethacrylate) (PMMA) (Figure S6). We stress that the combination of light, air, and moisture is essential to exploit all of these beneficial effects (Figures S7 and S8), but longer exposure times to this combination lead to degradation (Figure S9).[22,23]

Enhancements in Film Photoconductance and Diffusion Length

In order to assess the impact of the treatments on charge transport, we performed time-resolved microwave conductivity (TRMC) measurements. This technique monitors the photoconductance ΔG on pulsed illumination, giving a direct measure of the charge-carrier yield, lifetimes, and mobilities.[24,25] Figure 2A shows ΔG of the films after storage in dry air (untreated, black curve) and after light soaking for 30 min in humid air (40% relative humidity) under a white light LED source generating a similar photon flux to AM1.5 sunlight (treated, red) (see Figure S10 for other conditions). Importantly, we see a profound increase in the lifetime of the charge carriers after the treatment, which is retained even after storage of the bare film in a nitrogen glove box for a week (redried, blue curve).

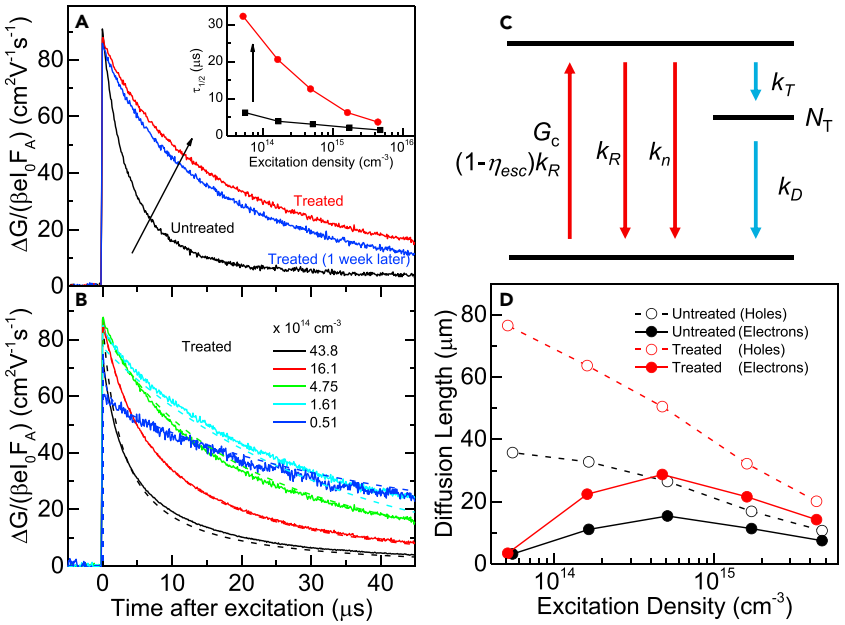

Figure 2. Enhancements in Film Photoconductance Determined from Time-Resolved Microwave Conductivity Measurements

(A) Photoconductance measurements for a $MAPbI_3$ film after storage in dry air and after being subjected to light soaking for 30 min in humid air (40% humidity) under a constant photon flux similar to solar conditions. The TRMC trace taken after storing the same sample in a nitrogen glove box for a week after the treatment is also shown. The TRMC decays were recorded by photo-exciting the samples in dry N_2 with pulsed illumination at 500 nm and an excitation density of $\sim 5 \times 10^{14}$ cm^{-3}.

(B and C) TRMC decays (normalized to absorbed flux) of the treated samples with the initial charge excitation density as indicated (B). Dashed lines are fits to the data using the trap model summarized in (C), where G_c is the generation rate and k_T and k_D are the trapping and trap depopulation rates, respectively.

(D) Diffusion lengths of the electrons and holes before and after the treatments.

See also Figures S10–S13, Tables 1 and S1.

In Figure 2B, we show TRMC decays of the treated films with initial photo-excited charge densities varying over three orders of magnitude (see Figure S11 for other treatments). The resulting half lifetimes of the excitation-dependent decays $\tau_{1/2}$ (time taken to decay to half of the initial value) for different excitation densities are shown in the inset of Figure 2A. Most importantly, we see a substantial increase in the lifetimes of the charge carriers at each excitation density in the treated film compared with the untreated film, with the lifetime at the lowest fluences increasing from 6.2 μs to 32.3 μs after treatment. We note that the lifetimes ($\sim$1–6 μs) and mobilities ($\mu \sim$ 70–90 $cm^2\ V^{-1}\ s^{-1}$) of carriers even in the untreated film are already as large as in the highest-quality perovskite thin films reported.[15,26]

We can describe the observed behavior based on a kinetic model that incorporates the presence of a density N_T of deep electron trap states and is summarized in Figure 2C (see Supplemental Information for details).[5,27] If the photo-excitation generation density exceeds the deep trap density N_T, the charge-carrier decay kinetics are dominated by bimolecular recombination of electrons and holes, but at low fluence when many electrons are immobilized into these trap states, the recombination appears pseudo-monomolecular.[5] Richter et al.[4] recently proposed that the bimolecular recombination constant is actually comprised of a radiative

Table 1. Summary of Parameters from TRMC Measurements and Fits for Thin Films of $MAPbI_3$ Untreated and Treated

Sample	$\mu_e + \mu_h$ ($cm^2\ V^{-1}\ s^{-1}$)	k_2^{eff} ($10^{-11}\ cm^3\ s^{-1}$)	η (%)	k_2^{int} ($10^{-11}\ cm^3\ s^{-1}$)
Untreated	87	26.0	1	26.2
Treated	87	7.60	84	28.5

Untreated: stored in dry air for 30 min. Treated: light soaked in humidified air for 30 min under white light equivalent to solar conditions. The PLQE values η are from Figure S1.

(k_R) and non-radiative (k_n) component. This leads to an effective (external) bimolecular recombination rate constant that can be extracted from fits to the TRMC data given by an expression encompassing the effects of photon recycling and light out-coupling:

$$k_2^{eff} = \eta_{esc} k_R + k_n, \qquad \text{(Equation 1)}$$

where η_{esc} = 12.7% is the escape probability of a photon from a bare perovskite film on glass for the film thickness in this work.[4]

We fit this model to the set of excitation-dependent decays and show the fits for the treated films as dashed lines in Figure 2B (see Figure S11 for other treatments, Tables 1 and S1 for parameters, and Supplemental Information for discussion on sensitivity of the analysis). We find a remarkably low deep trap density for these samples, which only changes negligibly for the sample light soaked in humid air ($N_t = 6.0 \times 10^{13}\ cm^{-3}$ reducing to $5.5 \times 10^{13}\ cm^{-3}$), suggesting that the treatments are primarily affecting the radiative and non-radiative components of the bimolecular recombination constant. Furthermore, the mobility values for the electrons and holes remain similar upon the treatment, indicating that the bulk properties have not changed significantly.

We find that the k_2^{eff} decreases from $26.0 \times 10^{-11}\ cm^3\ s^{-1}$ when untreated to $7.60 \times 10^{-11}\ cm^3\ s^{-1}$ with the treatment. With the measured internal PLQE η values, we extract the internal bimolecular rates k_2^{int}, which we find to be almost unchanged from the untreated ($26.2 \times 10^{-11}\ cm^3\ s^{-1}$) to treated ($28.5 \times 10^{-11}\ cm^3\ s^{-1}$) samples (see Supplemental Information for details). This suggests that the rate of recombination collisions between electrons and holes is unchanged on treatment. However, the treatments increase the fraction of these collisions that are radiative compared with the fractions that are non-radiative. This means that each carrier is more likely to be re-generated due to a photon recycling event,[28] which is only possible with radiative recombination, prolonging the effective lifetime of the carriers. This leads to the conclusion that the increase in carrier lifetimes with treatment is primarily due to an increased fraction of radiative recombination, in turn leading to enhanced recycling of carriers.

We use the kinetic model to extract the individual carrier lifetimes and use these to calculate the resulting diffusion lengths of each carrier using $L_D = \sqrt{k_B T \mu \tau_{1/2}/e}$, where k_B is the Boltzmann constant, T the temperature, e the electron charge, and μ the carrier mobility extracted from the photoconductance measurements (Figures 2D and S12).[12] We find remarkable hole diffusion lengths of 76.5 μm in the treated film at low excitation fluences at which the electron traps are still not completely saturated, and therefore the majority of the electrons are immobilized in trap states, while we find electron diffusion lengths reaching 28.7 μm at intermediate charge densities in which all of these electron traps are filled. We note that these diffusion lengths are the average cumulative distance that charges diffuse, including recycling through reabsorption events (Figure S13).

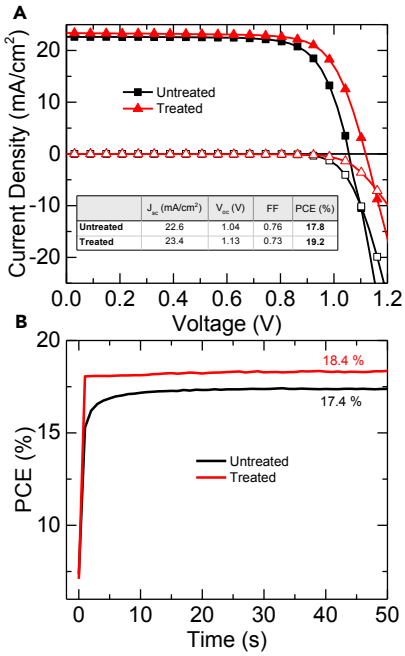

Figure 3. Enhancements in Solar Cell Device Performances

(A) Light and dark J-V curves of champion devices for the devices containing untreated (stored in dry air) and treated (light soaked in humid air) films measured under AM1.5 100 mW/cm^2 simulated sunlight.

(B) Stabilized power output of the devices presented in (A) measured by holding the devices at their maximum power point (as determined from J-V curves) for 50 s.

See also Figures S14–S20.

The exceptional diffusion lengths, carrier lifetimes, mobilities, and low deep trap densities show that these polycrystalline thin films possess properties only previously demonstrated in single crystals.[12,29] In fact, the lifetime ($\tau_{1/2}$ = 32.3 μs) of the treated film already exceeds that seen in single crystals under similar conditions (~15 μs), and the deep trap densities are comparably low.[12] The surface recombination velocity (SRV) in unpassivated perovskite polycrystalline films and single crystals has been reported to be ~1,000 cm/s,[30] which can be reduced to ~3 cm/s for passivated single crystals.[13] We calculate SRV ~ $L/2\tau_{1/2}$ ~ 0.4 cm/s for the holes at low charge densities in treated films in which $\tau_{1/2}$ = 32.3 μs and L = 250 nm is the film thickness (see Supplemental Information).[13,31] This is an order of magnitude lower than passivated perovskite single crystals and comparable with the lowest value ever reported for any semiconductor in <111> crystalline silicon (0.15 cm/s),[31,32] which is truly remarkable when considering that these are solution-processed polycrystalline films.

Enhancements in Solar Cell Device Performance

To validate the treatments in devices, we constructed planar heterojunction perovskite solar cell devices in the configuration of FTO (fluorinated tin oxide)/SnO_2/$CH_3NH_3PbI_3$/2,2′,7,7′-tetrakis(*N*,*N*′-di-*p*-methoxyphenylamine)-9,9′-spirobifluorene (spiro-OMeTAD)/Au, where the perovskite was deposited using an acetonitrile-based solution-processing route.[33] We performed the treatments on the bare perovskite in half-constructed devices before depositing the hole transporter (spiro-OMeTAD) and Au electrodes for testing. We show in Figure 3A the current-voltage (J-V) curves and in Figure 3B the stabilized power output of champion devices incorporating the untreated films and the treated films that have been exposed to humid air with light soaking for 20 min under a white light LED array similar to solar illumination conditions (see Figure S14 for other treatments and Figure S15 for device statistics). We see an increase in the short-circuit current from 22.6 to 23.4 mA/cm^2 and the open-circuit voltage from 1.04 to 1.13 V, both consistent with the reduction in non-radiative decay and subsequent increase in carrier diffusion length and lifetime

after the treatments. This yields champion device efficiencies of 19.2% (treated) and 17.8% (untreated), with stabilized power output of 18.4% and 17.4%, respectively. Although hysteresis is still present (Figure S14), we find that the extent of the hysteresis is reduced with the treatment and this finding is accompanied by a noticeable increase in the steady-state efficiency of the devices (Figure 3B). Importantly, the time to rise to stabilized power output is much faster in the treated film, with near-instant rise to stable output compared with the slower ~10–20 s rise in the untreated films with the same device structure (see Figure S16 for other treatments). These findings are consistent with the PL output in the treated films instantly reaching their maximum value without a slow rise time (cf. Figure 1G, inset). They are also consistent with the assertion that ionic migration, the origin of the slow transient rises,[34] is impeded in the devices with treated films. The device performance enhancements remain after 3 weeks of storage in a nitrogen glove box and still remain superior to the controls after 8 weeks of storage (Figure S17). We also find enhancements when using the acetate-based method (Figures S18–S20), suggesting that the post-treatments are capable of improving perovskite films processed in different ways. We note that the optically implied open-circuit voltages[35] from an internal quantum efficiency of 89% should lead to voltage losses of only a few meV, indicating that there are still non-radiative losses introduced from the contacts,[36] insufficient light out-coupling from the devices or partial removal of the treatment following deposition of the top layers. We also note that the light-soaking enhancements are not as evident when performed on the full device stack rather than the half stack, and we speculate that this is because the hole transporting layer prevents the crucial interaction of the atmospheric molecules with the perovskite surface.

DISCUSSION

Mechanism of Photobrightening

In order to explain the observations, we propose that there is a distribution of shallow surface states, and the carriers in the bands can easily transfer into and thermally out of these states (Figure 4A). We depict these as shallow electron states just below the conduction band, but these could equally be shallow hole states above the valence band. We propose that the radiative bimolecular recombination (k_R) is band-to-band recombination while the non-radiative bimolecular component (k_n) is electron-hole recombination mitigated through these shallow surface states (Figure 4A). If such states remained mostly unoccupied, this non-radiative recombination would be bimolecular because the rate would depend on the concentration of both electrons (and hence the density of trapped electrons) and holes. The treatments then decrease the density of these shallow states, leading to a greater fraction of electron-hole collision events being radiative k_R than non-radiative k_n and hence significantly increasing the PLQE (Figure 4A). We note that we distinguish these shallow states from the deep trap states, which solely mitigate non-radiative recombination through irreversible electron trapping and which are of very low density in the samples studied here ($N_t \sim 10^{13}$ cm^{-3}) and appear to be mostly unaffected by the treatments.

The nature of these shallow states that promote non-radiative recombination but do not affect charge mobility is unclear. Since the mobility and therefore bulk charge transport (including grain-to-grain transport) is mostly unaffected by the surface treatments, we propose that the shallow states primarily reside on the surfaces as opposed to the grain boundaries. However, we note that we cannot exclude the additional presence of deep traps and/or low densities of shallow traps on grain boundaries in the bulk. Here, we explore the case of a density of shallow defects

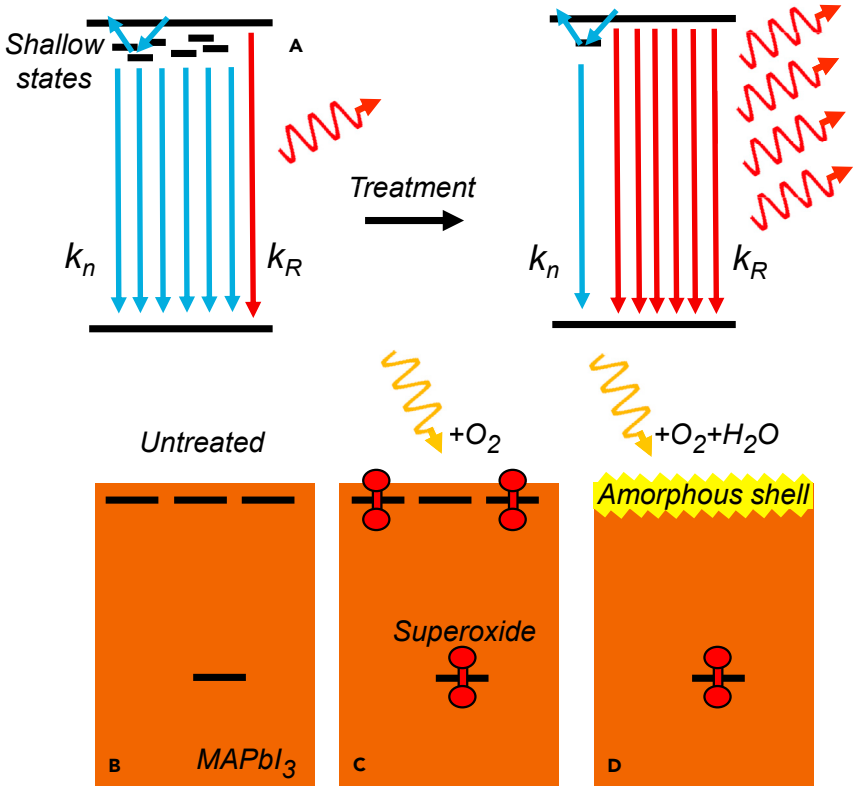

Figure 4. Mechanism of Photobrightening

(A) Schematic showing non-radiative recombination (k_n) dominating owing to shallow surface states, which are removed in the treatment to lead to radiative-dominant (k_R) recombination. (B–D) Untreated $MAPbI_3$ films (B) containing non-radiative trap states that are passivated by exposure of $MAPbI_3$ to (C) light and oxygen and (D) light, oxygen, and water.
See also Figures S23 and S24.

associated with iodide vacancies,[37] but we note that other explanations are also possible such as surface traps due to electron-phonon coupling[38] or surface structures with an indirect band gap.[24] Recently, we reported experimental and theoretical evidence that oxygen diffusion into $MAPbI_3$ films is accompanied by photo-induced formation of superoxide species (O_2^-) at iodide vacancies over the timescales relevant to the enhancements we report here.[23] Here, we use density functional theory calculations to show that, as a result of O_2 reduction to O_2^- at surface vacancies occupied by photogenerated electrons, the sub-gap states shift down into the valence band (Figure S21), removing the shallow states. The passivating effect of oxygen is consistent with an increase in surface oxygen content after the treatments (Figure S22).

We summarize the proposed mechanism for the treatments in Figures 4B–4D. First, an untreated $MAPbI_3$ sample containing surface states (Figure 4B) is exposed to light and oxygen. This reduces the density of surface states and leads to photobrightening (Figure 4C) through the formation of passivating superoxide species. This process is reversible on a timescale of hours if the sample is then kept in the dark. Second, when an untreated sample is briefly exposed to light, H_2O, and O_2 (Figure 4D), the density of shallow states decreases to an even greater extent due to complete removal of the states at the surface by forming a nanometer-thin amorphous shell of inert degradation products;[39] these shells could be indicated

by a minor texturing of the surfaces after the treatment (Figure S23) but no detectable changes in the crystalline properties of the surface (Figure S24). This process is mostly irreversible; the shell of degraded material acts as a containing barrier through which the oxygen species only slowly de-gas from the film (an encapsulating impermeable polymer such as PMMA is even more effective). The treatments inhibit ion migration, since oxygen occupies iodide vacancy sites involved in the migration process, and the degraded shell introduces a partial barrier to ionic transport in the intergrain regions.

We expect that further optimization of these scalable treatments, along with deeper understanding of the nature of these shallow surface states and resulting recombination pathways, will lead to solar and light-emitting device efficiencies approaching the theoretical limits with minimal ionic migration.

EXPERIMENTAL PROCEDURES

Sample Preparation

Glass substrates were washed sequentially with soap, de-ionized water, acetone, and isopropanol, and finally treated under oxygen plasma for 10 min. Thin films of $MAPbI_3$ were solution processed by employing a methylammonium iodide (MAI) and lead acetate $Pb(Ac)_2 \cdot 3H_2O$ precursor mixture with a hypophosporous acid (HPA) additive.[18] MAI (Dyesol) and $Pb(Ac)_2 \cdot 3H_2O$ (Sigma-Aldrich) were dissolved in anhydrous *N*,*N*-dimethylformamide (DMF) at a 3:1 molar ratio with final concentration of 37 wt % and HPA added to an HPA:Pb molar ratio of ~11%. The precursor solution was spin coated at 2,000 rpm for 45 s in a nitrogen-filled glove box, and the substrates were then dried at room temperature for 10 min before annealing at 100°C for 5 min. All samples were then stored in a nitrogen-filled glove box until used.

Macro-photoluminescence Measurements

PL measurements were acquired by photo-exciting perovskite films on coverslips enclosed in a custom-built flow chamber capable of flowing ultra-high purity gases in ultra-dry or controllably humidified form (~40%–50% relative humidity for all humidified measurements). The samples were photo-excited with a 532-nm CW laser at intensities approximately equivalent to the photon fluxes of ~2 sun irradiation (~150 mW/cm^2). The PL was collected using fiber-coupled collecting optics and the emission detected using an Ocean Optics USB4000 fiber-coupled spectrometer.

The external PL quantum efficiency (η_{meas}) was measured using an integrating sphere in a nitrogen-filled glove box using a 532-nm excitation laser at an illumination intensity of ~150 mW/cm^2. The PLQE was computed using well-established techniques.[40] The internal PLQE η was calculated by accounting for collection losses in the measured values η_{meas} due to photon recycling and poor light out-coupling at the perovskite/air and perovskite/glass interfaces, given by:

$$\eta = \eta \left[\frac{\eta_{esc}}{\eta_{meas}} - (\eta_{esc} - 1) \right]^{-1}, \qquad \text{(Equation 2)}$$

where η_{esc} = 12.7% is the escape probability of a photon from a bare perovskite film on glass for the film thickness in this work.[4] The PLQE measurements in other environments were then determined with respect to the PLQE values measured directly in dry nitrogen.

Macroscopic time-resolved PL measurements were obtained on the treated films in dry nitrogen using an Edinburgh LifeSpec spectrometer equipped with a

single-photon counter. The films were excited at 405 nm with a picosecond pulsed diode laser (Hamamatsu, M8903-01) at a repetition rate of 20 kHz.

Micro(Confocal)-photoluminescence Measurements

Confocal PL maps were acquired using a custom-built time-correlated single-photon counting confocal microscope (Nikon Eclipse Ti-E) set up with a 100× oil objective (Nikon CFI PlanApo Lambda, 1.45 NA). The samples were measured in the custom-built flow chamber with the desired gas and/or humidity level. The coverslip samples were photo-excited through the glass side using a 405 nm laser head (LDH-P-C-405, PicoQuant GmbH) with pulse duration of <90 ps, fluence of ~1 $\mu J/cm^2$/pulse, and a repetition rate of 0.5 MHz. The PL from the sample was collected by the same objective, and the resulting collimated beam passes through a long-pass filter with a cutoff at 416 nm (Semrock Inc., BLP01-405R-25) to remove any residual scattered or reflected excitation light. Light soaking was achieved by coupling a green 532-nm laser diode (Thorlabs) into the microscope, yielding a soaking spot size of ~10 μm and a power of ~1 μW. A single-photon detecting avalanche photodiode (APD) (MPD PDM Series 50 mm) was used for the detection. The sample was scanned using a piezoelectric scanning stage. The measurements were acquired using the commercial software SymphoTime 64 (PicoQuant GmbH).

Time-Resolved Microwave Conductivity Measurements

For the TRMC measurements, the treatments to the perovskite films were performed in a glove bag using controlled atmosphere and humidity. For light soaking, we applied an LED white light source (LuxSpot LS17-002D55) generating a similar number of photons in the visible as simulated sunlight (~100 mW/cm^2, AM1.5). The bag has two gas purges: one introduces dry gas and the other introduces a water bubbler that is connected to the gas source. The relative humidity was controlled to be ~40%–50% for any treatments involving humidity. The treatment time was fixed at 30 min for all. After the treatment, the samples were immediately transferred into a N_2 glove box and then mounted in a sealed microwave resonance cavity for TRMC measurements.

The TRMC technique monitors the change in reflected microwave power by the loaded microwave cavity upon pulsed laser excitation. The photoconductance (ΔG) of the samples was deduced from the measured laser-induced change in normalized microwave power ($\Delta P/P$) by

$$-K\Delta G(t) = \frac{\Delta P(t)}{P}, \qquad \text{(Equation 3)}$$

where K is the sensitivity factor. The yield of generated free charges φ and mobility $\sum\mu = (\mu_e + \mu_h)$ were obtained by:

$$\varphi \sum \mu = \frac{\Delta G}{I_0 \beta e F_A} \qquad \text{(Equation 4)}$$

where I_0 is the number of photons per pulse per unit area, β is a geometry constant of the microwave cell, e is the elementary charge, and F_A is the fraction of light absorbed by the sample at the excitation wavelength of 500 nm (0.73).

Device Fabrication and Characterization

FTO-coated glass sheets (7 Ω cm^{-1}; Hartford Glass) were etched with zinc powder and HCl (3 M) to obtain the required electrode pattern. The sheets were then washed with soap (2% Hellmanex in water), deionized water, acetone, and

isopropanol, and finally treated under oxygen plasma for 10 min to remove the last traces of organic residues. All chemicals were purchased from Sigma-Aldrich and used as received unless otherwise stated. A compact layer of SnO_2 was then deposited using a slight modification of the process reported by Anaraki et al.[41] A first layer of SnO_2 was deposited onto the cleaned FTO substrate by spin coating a layer of $SnCl_4 \cdot 5H_2O$ (17.5 mg/mL) diluted in anhydrous isopropanol (3,000 rpm), followed by annealing at 180°C for 60 min. The substrates were then immersed in an acidic chemical bath of $SnCl_2 \cdot 2H_2O$ for 180 min at 70°C. The substrates were then briefly sonicated in deionized water before being transferred to a hotplate and annealed at 180°C for a further 60 min, after which they were allowed to cool down naturally to room temperature. After cooling, a 0.5 M solution of 1:1.06 MAI (Dyesol) to PbI_2 (TCI Chemicals, 99% purity) in the ACN/MA solvent was prepared as described by Noel et al.[33] The solution was then spin coated onto the substrate at 2,000 rpm for 45 s in dry air, resulting in the formation of a smooth, dense, perovskite layer. The substrate was then heated at 100°C for 60 min. After annealing, the substrates were allowed to cool to room temperature. For lead-acetate-based devices, lead acetate trihydrate and methylammonium iodide were dissolved in DMF at a 1:3 molar ratio, such that the resulting solution was 30 wt % with respect to perovskite salts. Hypophosphorous acid was added according to the method described by Zhang et al.[18] The precursor solution was then spin coated onto the substrates at 2,000 rpm for 45 s in an inert atmosphere. The substrates were then dried at room temperature for 10 min before being annealed at 100°C for 5 min. After annealing, the substrates were allowed to cool down naturally to room temperature.

The light- and atmosphere-soaking treatments were performed on these half-constructed devices under the stated atmospheric conditions by illuminating with a white light LED array with an intensity similar to simulated sunlight for 20 min.

The hole transporting material spiro-OMeTAD was then dissolved in chlorobenzene with additives at a concentration of 30 mM lithium bis(trifluoromethanesulfonyl) imide and 80 mM tert-butylpyridine and spin coated at 2,000 rpm (45 s) on top of the samples in a nitrogen glove box. The devices were then stored in a dry air desiccator overnight before the deposition of the electrodes. Lastly, 80-nm-thick gold electrodes were evaporated onto the devices through a shadow mask, using a thermal evaporator. Devices were stored in nitrogen-filled glove box between measurements.

The current density-voltage (J-V) curves were measured (2400 Series SourceMeter, Keithley Instruments) under simulated AM 1.5 sunlight at 100 mW cm^{-2} irradiance generated by an Abet Class AAB sun 2000 simulator, with the intensity calibrated with an NREL calibrated KG5 filtered Si reference cell. The mismatch factor was calculated to be less than 1%. The solar cells were masked with a metal aperture to define the active area to be 0.0925 cm^2. The devices were held at 1.4 V under illumination for 5 s before the current-voltage scans were taken. The sweeps were taken from 1.4 V to 0 V, then from 0 V to 1.4 V. The scan rate was 0.15 V per second. All devices were tested under ambient conditions.

SUPPLEMENTAL INFORMATION

Supplemental Information includes Supplemental Experimental Procedures, 24 figures, 1 table, and 1 scheme and can be found with this article online at http://dx.doi.org/10.1016/j.joule.2017.08.006.

AUTHOR CONTRIBUTIONS

R.B., S.D.S., and F.N. performed and analyzed the PL measurements. D.G., E.M.H., and T.J.S. acquired and analyzed the TRMC data. N.K.N., supervised by H.J.S., performed and analyzed the device data. C.E. performed the DFT calculations and, along with M.S.I., interpreted the results and developed the mechanism. A.O. and S.K.P. performed the surface characterizations. S.D.S. and R.B. wrote the manuscript, and all authors gave editorial input. S.D.S. supervised the project. S.D.S, V.B., and R.H.F. obtained the funding.

ACKNOWLEDGMENTS

S.D.S. has received funding from the European Union's Seventh Framework Program (Marie Curie Actions) under REA grant number PIOF-GA-2013-622630. This work made use of the Shared Experimental Facilities supported in part by the MRSEC Program of the National Science Foundation (NSF) under award number MDR – 1419807. R.B. acknowledges support from the MIT Undergraduate Research Opportunities Program (UROP). A.O. acknowledges support from the NSF under grant no. 1605406 (EP/L000202). D.G. acknowledges the China Scholarship Council for funding, file no. 201504910812. The authors acknowledge funding from the Engineering and Physical Sciences Research Council (EPSRC) under EP/P02484X/1 and the Programme Grant EP/M005143/1. M.S.I. and C.E. acknowledge support from the EPSRC Program grant on Energy Materials (EP/KO16288) and the Archer HPC/MCC Consortium (EP/L000202). E.M.H. gratefully acknowledges the Netherlands Organization for Scientific Research (NWO) Echo number 712.014.007 for funding. The work was also partially supported by Eni S.p.A. via the Eni-MIT Solar Frontiers Center. The authors thank Mengfei Wu and Marc Baldo for access to an integrating sphere, Jay Patel and Michael Johnston for EQE verifications, and Eli Yablonovitch and Luis Pazos-Outón for helpful discussion.

Received: July 12, 2017
Revised: July 26, 2017
Accepted: August 8, 2017
Published: September 6, 2017

REFERENCES

1. Saliba, M., Matsui, T., Domanski, K., Seo, J.Y., Ummadisingu, A., Zakeeruddin, S.M., Correa-Baena, J.P., Tress, W.R., Abate, A., Hagfeldt, A., and Grätzel, M. (2016). Incorporation of rubidium cations into perovskite solar cells improves photovoltaic performance. Science *354*, 206–209.

2. Yang, W.S., Park, B.W., Jung, E.H., Jeon, N.J., Kim, Y.C., Lee, D.U., Shin, S.S., Seo, J., Kim, E.K., Noh, J.H., and Seok, S.I. (2017). Iodide management in formamidinium-lead-halide-based perovskite layers for efficient solar cells. Science *356*, 1376–1379.

3. Stranks, S.D. (2017). Nonradiative losses in metal halide perovskites. ACS Energy Lett. *2*, 1515–1525.

4. Richter, J.M., Abdi-Jalebi, M., Sadhanala, A., Tabachnyk, M., Rivett, J.P.H., Pazos-Outón, L.M., Gödel, K.C., Price, M., Deschler, F., and Friend, R.H. (2016). Enhancing photoluminescence yields in lead halide perovskites by photon recycling and light out-coupling. Nat. Commun. *7*, 13941.

5. Stranks, S.D., Burlakov, V.M., Leijtens, T., Ball, J.M., Goriely, A., and Snaith, H.J. (2014). Recombination kinetics in organic-inorganic perovskites: excitons, free charge, and subgap states. Phys. Rev. Appl. *2*, 034007.

6. Leijtens, T., Eperon, G.E., Barker, A.J., Grancini, G., Zhang, W., Ball, J.M., et al. (2016). Carrier trapping and recombination: the role of defect physics in enhancing the open circuit voltage of metal halide perovskite solar cells. Energy Environ Sci *9*, 3472–3481.

7. Wetzelaer, G.J., Scheepers, M., Sempere, A.M., Momblona, C., Avila, J., and Bolink, H.J. (2015). Trap-assisted non-radiative recombination in organic-inorganic perovskite solar cells. Adv. Mater. *27*, 1837–1841.

8. Miller, O.D., Yablonovitch, E., and Kurtz, S.R. (2012). Strong internal and external luminescence as solar cells approach the Shockley-Queisser limit. IEEE J. Photovolt *2*, 303–311.

9. Shi, D., Adinolfi, V., Comin, R., Yuan, M., Alarousu, E., Buin, A., Chen, Y., Hoogland, S., Rothenberger, A., Katsiev, K., et al. (2015). Low trap-state density and long carrier diffusion in organolead trihalide perovskite single crystals. Science *347*, 519–522.

10. Brenner, T.M., Egger, D.A., Kronik, L., Hodes, G., and Cahen, D. (2016). Hybrid organic—inorganic perovskites: low-cost semiconductors with intriguing charge-transport properties. Nat. Rev. Mater. *1*, 15007.

11. Nie, W., Tsai, H., Asadpour, R., Blancon, J.C., Neukirch, A.J., Gupta, G., Crochet, J.J., Chhowalla, M., Tretiak, S., Alam, M.A., et al. (2015). High-efficiency solution-processed perovskite solar cells with millimeter-scale grains. Science *347*, 522–525.

12. Bi, Y., Hutter, E.M., Fang, Y., Dong, Q., Huang, J., and Savenije, T.J. (2016). Charge carrier lifetimes exceeding 15 μs in methylammonium lead iodide single crystals. J. Phys. Chem. Lett. *7*, 923–928.

13. Fang, H.-H., Adjokatse, S., Wei, H., Yang, J., Blake, G.R., Huang, J., et al. (2016). Ultrahigh sensitivity of methylammonium lead tribromide

perovskite single crystals to environmental gases. Sci. Adv. *2*, e1600534.

14. Noel, N.K., Abate, A., Stranks, S.D., Parrott, E.S., Burlakov, V.M., Goriely, A., and Snaith, H.J. (2014). Enhanced photoluminescence and solar cell performance via Lewis base passivation of organic-inorganic lead halide perovskites. ACS Nano *8*, 9815–9821.

15. deQuilettes, D.W., Koch, S., Burke, S., Paranji, R.K., Shropshire, A.J., Ziffer, M.E., et al. (2016). Photoluminescence lifetimes exceeding 8 μs and quantum yields exceeding 30% in hybrid perovskite thin films by ligand passivation. ACS Energy Lett *1*, 438–444.

16. deQuilettes, D.W., Zhang, W., Burlakov, V.M., Graham, D.J., Leijtens, T., Osherov, A., Bulović, V., Snaith, H.J., Ginger, D.S., and Stranks, S.D. (2016). Photo-induced halide redistribution in organic-inorganic perovskite films. Nat. Commun. *7*, 11683.

17. Tian, Y., Peter, M., Unger, E., Abdellah, M., Zheng, K., Pullerits, T., Yartsev, A., Sundström, V., and Scheblykin, I.G. (2015). Mechanistic insights into perovskite photoluminescence enhancement: light curing with oxygen can boost yield thousandfold. Phys. Chem. Chem. Phys. *17*, 24978–24987.

18. Zhang, W., Pathak, S., Sakai, N., Stergiopoulos, T., Nayak, P.K., Noel, N.K., Haghighirad, A.A., Burlakov, V.M., deQuilettes, D.W., Sadhanala, A., et al. (2015). Enhanced optoelectronic quality of perovskite thin films with hypophosphorous acid for planar heterojunction solar cells. Nat. Commun. *6*, 10030.

19. Müller, C., Glaser, T., Plogmeyer, M., Sendner, M., Döring, S., Bakulin, A.A., et al. (2015). Water infiltration in methylammonium lead iodide perovskite: fast and inconspicuous. Chem. Mater. *27*, 7835–7841.

20. Eperon, G.E., Habisreutinger, S.N., Leijtens, T., Bruijnaers, B.J., van Franeker, J.J., deQuilettes, D.W., Pathak, S., Sutton, R.J., Grancini, G., Ginger, D.S., et al. (2015). The importance of moisture in hybrid lead halide perovskite thin film fabrication. ACS Nano *9*, 9380–9393.

21. Bass, K.K., McAnally, R.E., Zhou, S., Djurovich, P.I., Thompson, M.E., and Melot, B.C. (2014). Influence of moisture on the preparation, crystal structure, and photophysical properties of organohalide perovskites. Chem. Commun. *50*, 15819–15822.

22. Leguy, A.M.A., Hu, Y., Campoy-Quiles, M., Alonso, M.I., Weber, O.J., Azarhoosh, P., et al. (2015). Reversible hydration of CH3NH3PbI3 in films, single crystals, and solar cells. Chem. Mater. *27*, 3397–3407.

23. Aristidou, N., Eames, C., Sanchez-Molina, I., Bu, X., Kosco, J., Islam, M.S., and Haque, S.A. (2017). Fast oxygen diffusion and iodide defects mediate oxygen-induced degradation of perovskite solar cells. Nat. Commun. *8*, 15218.

24. Hutter, E.M., Gelvez-Rueda, M.C., Osherov, A., Bulovic, V., Grozema, F.C., Stranks, S.D., and Savenije, T.J. (2017). Direct-indirect character of the bandgap in methylammonium lead iodide perovskite. Nat. Mater. *16*, 115–120.

25. Reid, O.G., Yang, M., Kopidakis, N., Zhu, K., and Rumbles, G. (2016). Grain-size-limited mobility in methylammonium lead iodide perovskite thin films. ACS Energy Lett *1*, 561–565.

26. Johnston, M.B., and Herz, L.M. (2016). Hybrid perovskites for photovoltaics: charge-carrier recombination, diffusion, and radiative efficiencies. Acc. Chem. Res. *49*, 146–154.

27. Hutter, E.M., Eperon, G.E., Stranks, S.D., and Savenije, T.J. (2015). Charge carriers in planar and meso-structured organic-inorganic perovskites: mobilities, lifetimes, and concentrations of trap states. J. Phys. Chem. Lett. *6*, 3082–3090.

28. Pazos-Outón, L.M., Szumilo, M., Lamboll, R., Richter, J.M., Crespo-Quesada, M., Abdi-Jalebi, M., Beeson, H.J., Vrućinić, M., Alsari, M., Snaith, H.J., et al. (2016). Photon recycling in lead iodide perovskite solar cells. Science *351*, 1430–1433.

29. Chen, Y., Yi, H.T., Wu, X., Haroldson, R., Gartstein, Y.N., Rodionov, Y.I., Tikhonov, K.S., Zakhidov, A., Zhu, X.Y., and Podzorov, V. (2016). Extended carrier lifetimes and diffusion in hybrid perovskites revealed by Hall effect and photoconductivity measurements. Nat. Commun. *7*, 12253.

30. Yang, Y., Yang, M., Moore, D.T., Yan, Y., Miller, E.M., Zhu, K., et al. (2017). Top and bottom surfaces limit carrier lifetime in lead iodide perovskite films. Nat. Energy *2*, 16207.

31. Yablonovitch, E., Allara, D.L., Chang, C.C., Gmitter, T., and Bright, T.B. (1986). Unusually low surface-recombination velocity on silicon and germanium surfaces. Phys. Rev. Lett. *57*, 249–252.

32. Bonilla, R.S., Woodcock, F., and Wilshaw, P.R. (2014). Very low surface recombination velocity in n-type c-Si using extrinsic field effect passivation. J. Appl. Phys. *116*, 054102.

33. Noel, N.K., Habisreutinger, S.N., Wenger, B., Klug, M.T., Hörantner, M.T., Johnston, M.B., et al. (2017). A low viscosity, low boiling point, clean solvent system for the rapid crystallisation of highly specular perovskite films. Energy Environ Sci *10*, 145–152.

34. Eames, C., Frost, J.M., Barnes, P.R., O'Regan, B.C., Walsh, A., and Islam, M.S. (2015). Ionic transport in hybrid lead iodide perovskite solar cells. Nat. Commun. *6*, 7497.

35. Sutter-Fella, C.M., Li, Y., Amani, M., Ager, J.W., Toma, F.M., Yablonovitch, E., Sharp, I.D., and Javey, A. (2016). High photoluminescence quantum yield in band gap tunable bromide containing mixed halide perovskites. Nano Lett. *16*, 800–806.

36. Eperon, G.E., Moerman, D., and Ginger, D.S. (2016). Anticorrelation between local photoluminescence and photocurrent suggests variability in contact to active layer in perovskite solar cells. ACS Nano *10*, 10258–10266.

37. Yin, W.-J., Shi, T., and Yan, Y. (2014). Unusual defect physics in CH3NH3PbI3 perovskite solar cell absorber. Appl. Phys. Lett. *104*, 063903.

38. Wu, X., Trinh, M.T., Niesner, D., Zhu, H., Norman, Z., Owen, J.S., Yaffe, O., Kudisch, B.J., and Zhu, X.Y. (2015). Trap states in lead iodide perovskites. J. Am. Chem. Soc. *137*, 2089–2096.

39. Huang, W., Manser, J.S., Kamat, P.V., and Ptasinska, S. (2016). Evolution of chemical composition, morphology, and photovoltaic efficiency of CH3NH3PbI3 perovskite under ambient conditions. Chem. Mater. *28*, 303–311.

40. de Mello, J.C., Wittmann, H.F., and Friend, R.H. (1997). An improved experimental determination of external photoluminescence quantum efficiency. Adv. Mater. *9*, 230–232.

41. Anaraki, E.H., Kermanpur, A., Steier, L., Domanski, K., Matsui, T., Tress, W., Saliba, M., Abate, A., Grätzel, M., Hagfeldt, A., et al. (2016). Highly efficient and stable planar perovskite solar cells by solution-processed tin oxide. Energy Environ Sci *9*, 3128–3134.